1999-10

Numerical study of damage growth in particulate composites

Kwon, Y.W.; Liu, C.T.

Transactions of the ASME

Y.W. Kwon, C.T. Liu "Numerical study of damage growth in particulate composites." Journal of Engineering Materials and Technology, October 1999, Vol. 121/476-482.
https://hdl.handle.net/10945/57377

Numerical Study of Damage Growth in Particulate Composites

Y. W. Kwon
Mechanical Engineering Department,
Naval Postgraduate School,
Monterey, CA 93943

C. T. Liu
Phillips Laboratory,
Edwards AFB, CA 93524

A numerical study was conducted to simulate and predict damage initiation and growth around the crack tip in particulate composite specimens made of hard particles embedded in a soft rubber-like matrix material. Therefore, damage evolution in the matrix material around crack tips was investigated. The progressive damage was modeled using a micro/macro-approach which combined two levels of analyses like the micro-level and the macro-level analyses. Damage description was undertaken at the microlevel using a simplified three-dimensional unit-cell model and an isotropic continuum damage theory. The numerical study examined both thin and thick specimens with a short or long edge crack to understand the effects of specimen thickness and crack size on the damage initiation, growth, and saturation. Numerical results were compared with experimental data.

Introduction

There are many different kinds of particulate composite materials depending on the composition of the particles and the binding matrices. In general, damage modes of particulate composites can be classified into three cases such as particle cracking, matrix cracking, and particle/matrix interface debonding. The actual damage occurring in a particulate composite is governed by the stiffness and strength of the particles, binding matrix, and the interface. The particulate composite under study has hard particles embedded in a soft rubber-like matrix material. As a result, the composite has matrix cracking and interface debonding, but no particle cracking. This was confirmed by experimental observation using the Scanning Electron Microscope (SEM) (Cornwell and Schapery, 1975). Both matrix cracking and interface debonding are called matrix damage in the following discussion.

The effect of damage evolution in the matrix material was investigated on particle reinforced rubber-like composites. Nonlinear constitutive equations were developed to incorporate the damage evolution (Anderson and Farris, 1988; Farris, 1968; Gurtin and Francis, 1981; Knauss et al., 1973; Ravichandran and Liu, 1995; Shapery, 1982, 1986, 1991). Matrix damage caused an increase in volume dilatation. Therefore, those theories were developed to describe the nonlinear stress-strain curves using the change in volume dilatation. Most of the studies considered the uniaxial response even though they contained features which could be extended into multi-axial responses.

Progressive damage in the hard particle filled rubber-like matrix materials was studied around circular notches to investigate the crack initiation and propagation. Crack initiation and growth at circular notch tips were numerically modeled and predicted. The numerical results were validated using the experimental data (Kwon and Baron, 1998; Kwon et al., 1997; Kwon and Liu, 1997).

Both experimental and numerical studies were also conducted to examine the near crack tip behavior including the matrix damage (Liu and Ravichandran, 1997; Liu and Smith, 1996; Smith et al., 1990). Those studies measured and/or computed strain fields near the crack tips under different strain (loading) rates or different temperatures for the crack propagation tests. They did not explicitly report progressive damage other than its implicit effect on the strain fields.

The objective of the present study is to investigate the damage evolution around crack tips of thin and thick specimens made of a hard particle filled rubber-like matrix composite with a short or a long edge crack. Thus, the effects of specimen thickness and crack size on the damage evolution near the crack tip are studied using a micro/macro-approach. The study shows damage initiation, growth and saturation near the crack tip. The numerical results are compared to experimental data.

Micro/Macro-Approach

The analysis technique used for the present study is called a micro/macro-approach which couples two different levels of analyses in composites: micro-level analysis and macro-level analysis. The two levels of analyses have very different sizes in geometric dimensions. The macro-level has a dimension of composite specimens or structures while the micro-level has a dimension of embedded particles. The macro-level analysis is conducted using the Finite Element Method (FEM) so that a general shape of specimen, like cracked plates as used in the present study, can be analyzed. For the micro-level analysis, a simplified three-dimensional unit-cell model is utilized.

The interaction of the two analyses is shown in Fig. 1 and explained below. The micro-analysis interacts with finite elements of the macro-analysis. The micro-analysis provides the macro-analysis with effective composite material properties. The effective properties degrade as damage progresses in the matrix material. Thus, the effective properties must be recalculated in the micro-analysis along with progressive damage.

Using the effective properties, the macro-analysis is conducted in order to computes the composite strains (or called macro-strains). The micro-analysis decomposes the composite strains into micro-strains (stresses) in the matrix material. An isotropic damage theory is applied to the micro-strains (stresses) in the matrix material in order to determine the damage state and the degraded material properties of the matrix. Using the degraded matrix properties, the degraded effective composite properties are computed in the micro-analysis and used for the next macro-analysis.

The micro/macro-approach (sometimes called a local/global approach) was used in the past (Murthy and Chamis, 1984; Renard, 1990; Pecknold, 1990). Some of the works (for example, Renard, 1990) used a very detailed micromodel such as a refined 2-D finite element mesh of the representative micromodel which usually

Contributed by the Materials Division for publication in the JOURNAL OF ENGINEERING MATERIALS AND TECHNOLOGY. Manuscript received by the Materials Division January 15, 1999; revised manuscript received May 17, 1999. Guest Editors: Assimina A. Pelegri, Ann M. Sastry, and Robert Wetherhold.

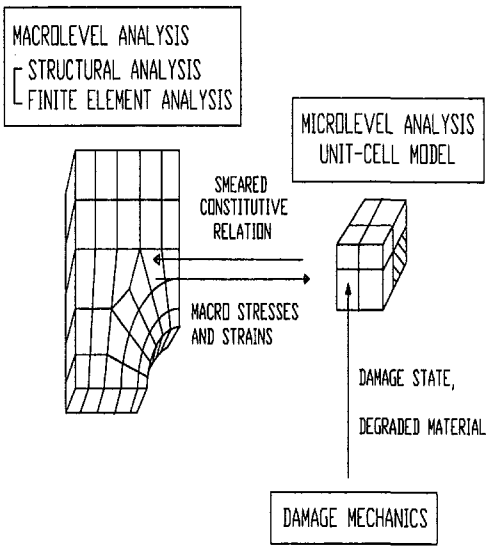

Fig. 1 Interactive micro/macro-approach

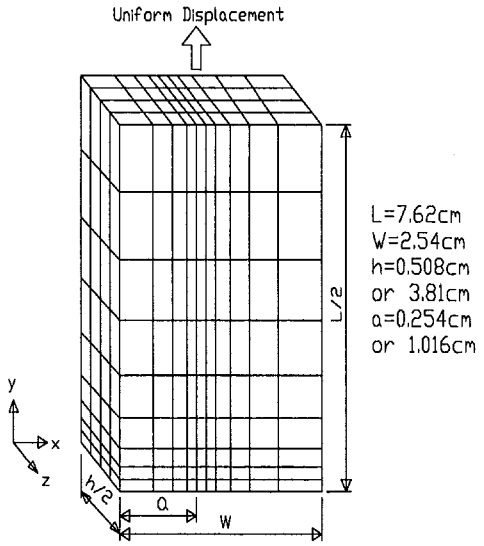

Fig. 2 Precracked specimen geometry with finite element mesh

consisted of a single fiber embedded in a square matrix domain. This model is computationally very expensive because the micro-level analysis should be conducted for every macro-level finite element with possible damage and it should be also repeated for the same element as damage evolves. Especially, three-dimensional analyses at both micro-level and macro-level require the approach impractical.

In order to make the micro/macro-approach more practical, the micromodel should be simplified. In this aspect, the homogenization technique would be useful. Various homogenization techniques have been developed to determine the effective material properties of composites using their constituent material and geometric properties. There has been an extensive work in this area so that all the references can not be compiled here. A few of them are given in the references (Devries et al., 1989; Felice and Rizzi, 1997; Siboni and Benveniste, 1991; Gibson, 1994). One of the techniques is called the unit cell method (Aboudi, 1987, 1989). The unit cell model was modified and used in this study. First of all, the derivation of the model was simplified mathematically. While the original unit cell model was based on the displacement fields within each subcell, the present model used strains and stresses directly. This simplified the development significantly but did not sacrifice the accuracy when the two models were compared with other experimental data (Kwon, 1993). Furthermore, the present model can decompose the macro-strains (stresses) into micro-strains (stresses) explicitly. This is one of the important features for the micro/macro-approach because the approach needs the two-way communication between the two levels of analyses. Finally, the unit cell model was divided into eight subcells because the model was applied to a particulate composite. The detailed discussion of the micro- and macro-model is given below:

Macro-Analysis. Because of its general applicability to complex problems, the finite element technique is adopted for the macro-analysis. The specimens under study are rectangular plates or solids with a single edge crack as shown in Fig. 2. Because of symmetry, the figure shows a quarter of the specimen with symmetric planes on the bottom side and the back side of Fig. 2. On each symmetric plane, its normal displacement is constrained. That is, z-displacement on the back plane and y-displacement on the bottom plane except for the crack face of Fig. 2 are constrained due to symmetry. In order to prevent the rigid body motion in the x-direction, one nodal point is also constrained along the x-axis. The geometric dimensions are provided in the figure.

The effective material properties computed from the micro-analysis are used to compute the element stiffness matrices. Because isoparametric elements are used in the present study, the material properties are supplied to Gauss quadrature points of each finite element for numerical integration. As a result, the micro-analysis is connected to Gauss quadrature points of the macro-level finite element model. This approach was also adopted in previous works (Haj-Ali, 1996; Pecknold and Rahman, 1994).

An incremental load or displacement is applied to the finite element analysis in order to capture progressive damage in the specimens. For each incremental load or displacement, the finite element analysis computes strains at the Gauss quadrature points. The strains are the composite level strains (macro-strains), i.e., smeared strains of the particles and the matrix. These strains are provided to the micro-analysis.

Micro-Analysis. When the macro-strains are provided to the micro-analysis, a micro-analysis is conducted to determine the micro-strains (strains at the particles and the matrix) and the micro-stresses. Because the macro-strains calculated at each integration point can represent the strain level around the point, the micro-model used for the analysis represents the particles and the matrix around each Gauss quadrature point. Thus, many individual shapes of particles and the binding matrix material around the integration point are smeared into a simple shape of a unit-cell model for the average behavior.

A three-dimensional micromodel for a particulate composite is shown in Fig. 3(a). A clear view of subcell locations is illustrated in Fig. 3(b). For a particulate composite, let subcell 1 denote the particle subcell and the rest be the binder matrix subcells. Planes 1–2, 2–3, and 3–1 are symmetric planes. Thus, a one-eighth section of the full unit-cell model is shown in the figure. In the model, the particle subcell is a cube with its side dimension equal to a one-third power of the particle volume fraction. The other subcells are sized accordingly because each side dimension in Fig. 3(a) is unity.

An incremental formulation is used in the following derivation. For mathematical simplicity, it is assumed that stress and strain components are constant within each subcell, respectively. (Subcell stresses and strains are micro-stresses and micro-strains.) Equilibrium of subcell stress increments at all interfaces satisfies

$$\Delta\sigma_{11}^{1} = \Delta\sigma_{11}^{2} \quad \Delta\sigma_{11}^{3} = \Delta\sigma_{11}^{4}$$

$$\Delta\sigma_{11}^{5} = \Delta\sigma_{11}^{6} \quad \Delta\sigma_{11}^{7} = \Delta\sigma_{11}^{8} \tag{1}$$

$$\Delta\sigma_{22}^{1} = \Delta\sigma_{22}^{3} \quad \Delta\sigma_{22}^{2} = \Delta\sigma_{22}^{4}$$

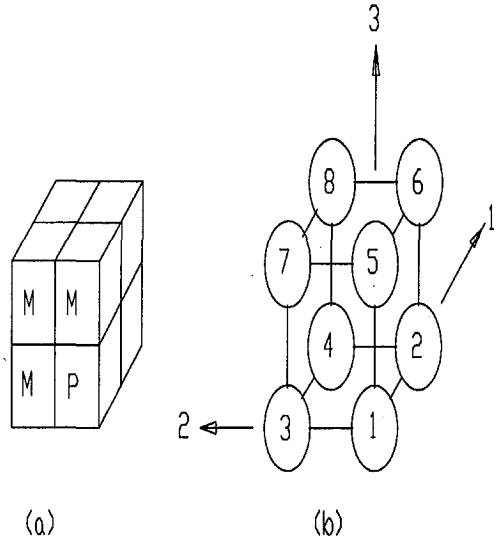

Fig. 3 Micromechanical unit-cell model

$$\Delta\sigma_{22}^{5} = \Delta\sigma_{22}^{7} \quad \Delta\sigma_{22}^{6} = \Delta\sigma_{22}^{8} \tag{2}$$

$$\Delta\sigma_{33}^{1} = \Delta\sigma_{33}^{5} \quad \Delta\sigma_{33}^{2} = \Delta\sigma_{33}^{6}$$

$$\Delta\sigma_{33}^{3} = \Delta\sigma_{33}^{7} \quad \Delta\sigma_{33}^{4} = \Delta\sigma_{33}^{8} \tag{3}$$

where the subscripts denote stress components along the axes shown in Fig. 3, and the superscript indicates the subcell number. It is assumed that each subcell material is orthotropic or isotropic so that normal stress/strain components are not coupled with shear components. The present development is presented for the normal components of stresses/strains. However, a similar development can be made for shearing stresses/strains but not presented here for brevity.

It is assumed that subcells satisfy the following strain compatibility:

$$l_p\Delta\epsilon_{11}^{1} + l_m\Delta\epsilon_{11}^{2} = l_p\Delta\epsilon_{11}^{3} + l_m\Delta\epsilon_{11}^{4} = l_p\Delta\epsilon_{11}^{5} + l_m\Delta\epsilon_{11}^{6} = l_p\Delta\epsilon_{11}^{7} + l_m\Delta\epsilon_{11}^{8} \tag{4}$$

$$d_p\Delta\epsilon_{22}^{1} + d_m\Delta\epsilon_{22}^{3} = d_p\Delta\epsilon_{22}^{2} + d_m\Delta\epsilon_{22}^{4} = d_p\Delta\epsilon_{22}^{5} + d_m\Delta\epsilon_{22}^{7} = d_p\Delta\epsilon_{22}^{6} + d_m\Delta\epsilon_{22}^{8} \tag{5}$$

$$d_p\Delta\epsilon_{33}^{1} + d_m\Delta\epsilon_{33}^{5} = d_p\Delta\epsilon_{33}^{2} + d_m\Delta\epsilon_{33}^{6} = d_p\Delta\epsilon_{33}^{3} + d_m\Delta\epsilon_{33}^{7} = d_p\Delta\epsilon_{33}^{4} + d_m\Delta\epsilon_{33}^{8} \tag{6}$$

in which l_p, l_m, d_p, and d_m are defined as

$$d_p = l_p = V_p^{1/3} \quad \text{and} \quad d_m = l_m = 1 - d_p \tag{7}$$

Here V_p is the particle volume fraction.

Each subcell has the constitutive equation

$$\Delta\sigma_{ij}^{n} = E_{ijkl}^{n}\Delta\epsilon_{kl}^{n} \tag{8}$$

in which E_{ijkl}^{n} is the material property tensor. The subscripts i, j, k and l vary from 1 to 3 while the superscript n changes from 1 to 8 for the present development, unless otherwise mentioned. The particle material under study shows elastic deformation while the matrix material exhibits viscoelastic deformation. As the first approximation, both materials are assumed to be elastic with the generalized Hooke's law. As damage evolves, the elastic material properties degrade as discussed in the next section.

The unit-cell stress and strain increments are computed from the volume average of subcell stress and strain increments.

$$\Delta\bar{\sigma}_{ij} = \sum_{n=1}^{8} V^n\Delta\sigma_{ij}^{n} \tag{9}$$

and

$$\Delta\bar{\epsilon}_{ij} = \sum_{n=1}^{8} V^n\Delta\epsilon_{ij}^{n} \tag{10}$$

Here, V^n is the volume fraction of the nth subcell. $\Delta\bar{\sigma}_{ij}$ and $\Delta\bar{\epsilon}_{ij}$ are the average unit-cell stress and strain (macro-stress and strain) increments, respectively. Further, the constitutive equation of the macro-stress and strain increments is

$$\Delta\bar{\sigma}_{ij} = \bar{E}_{ijkl}\Delta\bar{\epsilon}_{kl} \tag{11}$$

in which $\bar{E}_{ijkl}$ represents the effective material property tensor of the composite.

In order to correlate the constituent material behaviors to the effective material behavior, an algebraic manipulation of Eqs. (1)-(6), (8), and (10) is undertaken. First of all, Eq. (8) is substituted into Eqs. (1)-(3). The resultant equations show relations among subcell strains. Writing these equations plus Eqs. (4)-(6) and (10) in matrix form yields the expression

$$[T]\{\Delta\epsilon\} = \{f\} \tag{12}$$

in which $[T]$ is the matrix consisting of E_{ijkl}^{n} and geometric measures like V^n, d_p, d_m, l_p, and l_m as defined in Eq. (7). $\{\Delta\epsilon\}$ is the vector consisting of strain increments of the eight subcells. In addition, vector $\{f\}$ consists of two subvectors as given below:

$$\{f\}^T = \{\{0\}^T\{\Delta\bar{\epsilon}\}^T\} \tag{13}$$

where $\{0\}$ is the null vector, and $\{\Delta\bar{\epsilon}\}$ is the vector consisting of effective strain increments.

Inverting matrix $[T]$ and premultiplying it to Eq. (12) yields

$$\{\Delta\epsilon\} = [R]\{f\} = [R_2]\{\Delta\bar{\epsilon}\} \tag{14}$$

where

$$[R] = [T]^{-1} = [[R_1][R_2]] \tag{15}$$

Equation (9) can be rewritten in matrix form.

$$\{\Delta\bar{\sigma}\} = [V]\{\Delta\sigma\} \tag{16}$$

where $\{\Delta\bar{\sigma}\}$ is the vector consisting of the effective unit-cell stress increments and $\{\Delta\sigma\}$ is the vector containing subcell stress increments. $[V]$ is the matrix composed of subcell volume fractions. Equation (8) can be rewritten in matrix form as

$$\{\Delta\sigma\} = [E]\{\Delta\epsilon\} \tag{17}$$

where $[E]$ is the matrix consisting of E_{ijkl}^{n}.

Substitution of Eq. (17) into Eq. (16) results in

$$\{\Delta\bar{\sigma}\} = [V][E]\{\Delta\epsilon\} \tag{18}$$

Finally, use of Eq. (14) along with Eq. (18) gives the constitutive equation between unit-cell stresses and unit-cell strains.

$$\{\Delta\bar{\sigma}\} = [V][E][R_2]\{\Delta\bar{\epsilon}\} \tag{19}$$

Comparing Eq. (19) to Eq. (11) gives the effective material property matrix as shown below:

$$[\bar{E}] = [V][E][R_2] \tag{20}$$

For the micro-analysis, Eqs. (8), (14), and (20) are the key expressions. Equation (20) computes the effective composite material properties from the particle and matrix properties. These values are used for the macro-analysis. On the other hand, the macro-strains from the macro-analysis are applied to Eqs. (14) and

(8) so that the micro-strains and micro-stresses can be computed. The micro-strains and micro-stresses at the matrix material are used to determine the state of damage in the material using a continuum damage theory.

Damage Theory. Because the micromodel does not take account of the specific particle reinforcement geometry and particle spacing, local stresses at the microlevel (such as stress concentration caused by the specific shapes of particles and their spacing) cannot be determined. There is no way to compute such stresses unless all the specific informations are given. Even if those informations are known, it is practically impossible to model such a detail at the microlevel because of the very large number of particles and their random variation in terms of geometry and spacing.

As a result, the micro-strain (stress) obtained from the micromodel can be interpreted as the average value of a local area which was represented by the micromodel. In other words, the microstress is the average stress on the particles or the matrix within the zone represented by each Gauss integration point of every finite element, respectively. Then, a continuum damage theory is applied to the micro-strains and micro-stresses in order to determine the state of damage of each local zone and the average degraded material properties based on the damage amount. Thus, damage initiation, growth, and saturation are described using the damage theory. Even though the damage state may be anisotropic, an isotropic damage theory is used for mathematical simplicity with an assumption that random anisotropic damage distribution caused by random particle geometry and spacing can be approximated by an isotropic damage. Hence, the continuum damage theory developed in Simo and Ju (1987) was used in this study. Further discussion of the damage model is omitted here for brevity of the paper. (See Simo and Ju, 1987 for details.)

Results and Discussion

Four different numerical specimens were considered in this study. The geometric and loading conditions of the specimens were based on the previous experimental work conducted at the Air Force Research Laboratory under the supervision of one of the authors. The numerical results were compared to the experimental data, and they were also used to understand and explain the observation during the experiment.

All the specimens were $L = 7.62$ cm (3 in.) long and $W = 2.54$ cm (1 in.) wide with a single edge crack located in the middle of the specimens lengthwise as seen in Fig. 2. The thickness and crack size were varied. Two specimens were $h = 0.508$ cm (0.2 in.) thick and the other two were $h = 3.81$ cm (1.5 in.) thick. The formers are called thin specimens while the latters are called thick specimens in the following discussion. Further, one of the two had a short crack of $a = 0.254$ cm (0.1 in.) and the other had a long crack of $a = 1.016$ cm (0.4 in.) for both thin and thick specimens, respectively. Therefore, the effects of the specimen thickness and the crack size were evaluated on the damage initiation and growth in the matrix material around the crack tips.

Because of bisymmetry, a quarter of the specimen was modeled. A typical finite element mesh is shown in Fig. 2 with eight-node solid elements. The actual mesh size was determined from a numerical convergency test within the capacity of the computer (SGI workstation). A uniform vertical displacement was applied to the top plane of the quarter specimen as shown in Fig. 2. That is, the displacement (strain) control was used in the analysis like the physical testing. The displacement (strain) was applied incrementally to compute progressive damage. The stress-strain curve obtained from the numerical study was compared to the experimental curve in Fig. 4 as damage initiated and grew for an uncracked specimen. The two curves compare very well. Even for a cracked specimen, the average stress-strain curves agreed well, too.

The first case was the thick specimen with a long edge crack. The thickness effect was studied with this specimen. Therefore, the present study examined the variation of damage as well as stress (strain) fields through the specimen thickness. For the thick specimen, the center zone (back xy-plane in Fig. 2) is close to the plane strain condition while the free surface (front xy-plane in Fig. 2) is under the plane stress condition. The plane strain condition has a higher tri-axial state than the plane stress condition.

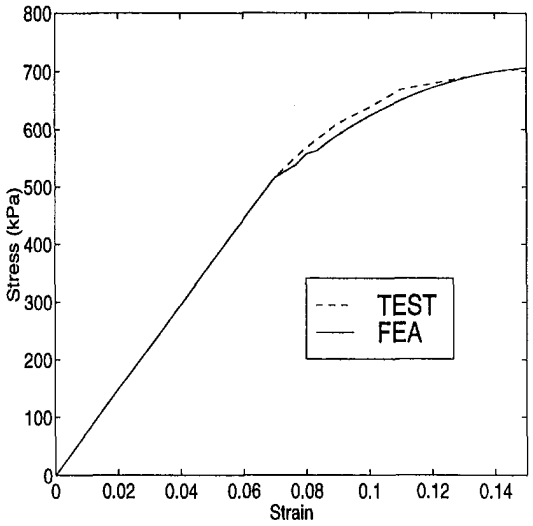

Fig. 4 Plot of stress-strain curves

An experimental study indicated that the composite material under study showed progressive damage under the tri-axial state of stresses. As a result, the plane strain condition results in a greater damage than the plane stress condition. In other words, damage is greater at the center of the specimen thickness than at the free surface as seen in Fig. 5. The figure shows the initiation, growth, and saturation of damage at the crack tip elements which are the elements located at the crack tip. In the figure, the damage parameter is plotted for applied strains along the thickness direction, $Z = 2z/h$, where h is the specimen thickness. The damage parameter is zero before damage initiation and close to unity as damage saturates. Damage is the largest at the center ($Z = 0$ in Fig. 5) and the smallest at the free surface ($Z = 1.0$). There is a gradient in the damage distribution along the thickness. However, there is a smaller damage gradient around the center than around the free surface. As the damage saturates (i.e., the damage parameter

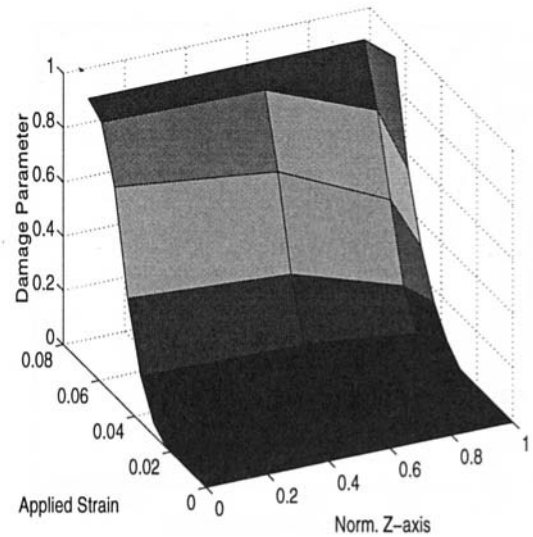

Fig. 5 Plot of damage growth versus applied strain at crack tip elements along the thickness of the thick specimen with a long crack

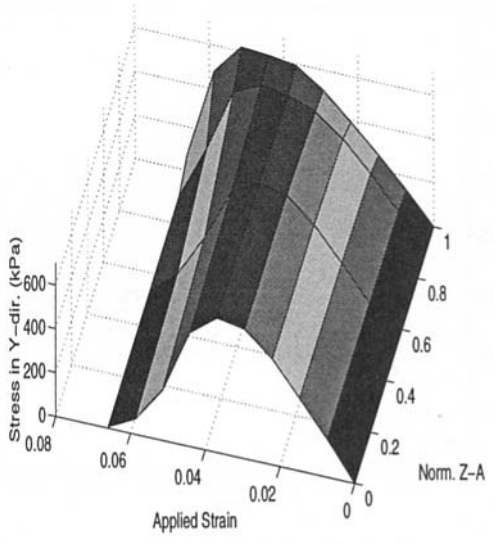

Fig. 6 Plot of stress σ_y versus applied strain at crack tip elements along the thickness of the thick specimen with a long crack

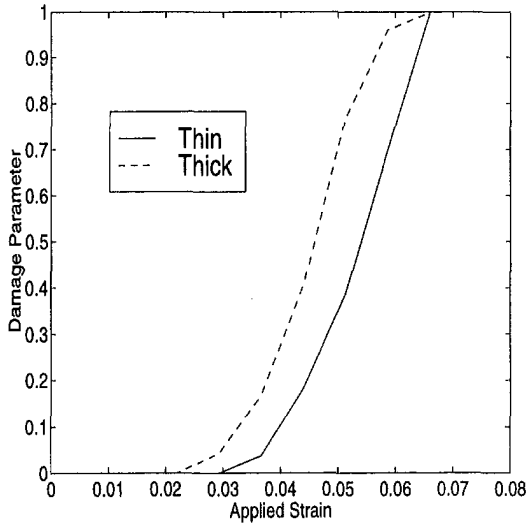

Fig. 8 Plot of damage growth versus applied strain for both thin and thick specimens with a long crack

approaches unity), the damage becomes constant through the thickness except for very near the free surface. However, the free edge is also close to damage saturation. Thus, the numerical result indicates an almost uniform damage saturation through the thickness.

Figure 6 plots the stress σ_y at the crack tip elements for the applied strains. Before any major damage in the matrix material, the stress is largest at the center and the smallest at the free surface. As the damage is also higher at the center, the stress at the center drops first with increasing damage. Therefore, the stress becomes larger away from the center, eventually at the free surface. As damage approaches saturation, the stress drops to a very small value across the thickness. In other words, if the damage saturates in a material, the material cannot support any external load. Since the crack tip element cannot sustain the applied load with damage saturation, the saturation point is considered as the onset of crack propagation. Based on this assumption, Figs. 5 and 6 predict uniform crack propagation at the crack tip elements. The experimental study also showed uniform crack propagation of the thick specimen confirming the numerical result.

Figure 7 shows the damage distribution in front of the crack tip at the onset of damage saturation. The distance from the crack tip was normalized with respect to the specimen width. As seen in the figure, the intensive damage is confined within a small zone from the crack tip at the center as well as at the free surface. The experiment also confirmed this observation qualitatively.

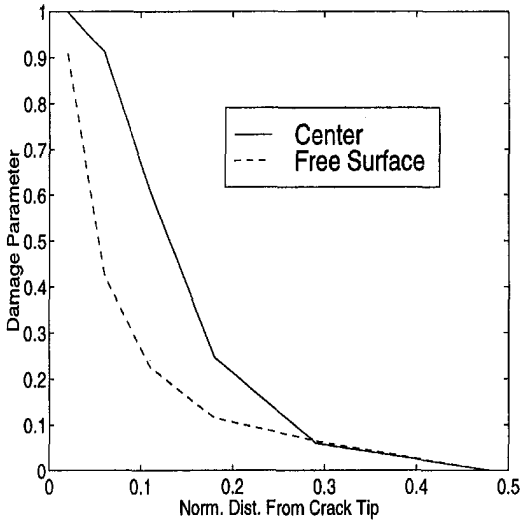

Fig. 7 Damage distribution in front of crack tip for the thick specimens with a long crack

The next study was for the thin specimen with a long crack. The results of the thin specimen were compared with those of the previous thick specimen. As expected, the thin specimen has the more prevailing plane stress condition through the thickness than the thick specimen so that the damage occurs very uniformly through the thickness. The damage evolution in the crack tip element of the thin specimen is plotted in Fig. 8 and compared to that in the thick specimen. The damage initiates later (i.e., at a larger applied strain level) for the thin specimen than the thick specimen. However, damage growth rate is greater for the thin specimen so that the damage saturation occurs at the same applied strain level as that for the thick specimen. This result is different from a metallic material as stated in (Knott, 1973). An aluminum alloy showed an increasing fracture toughness for a thiner specimen until the specimen became very thin. The experimental data also showed the onset of crack propagation at the same applied strain level for both the thick and thin specimens. The levels of applied strains at the onset of crack growth agreed between the experimental and numerical data with less than a ten percent difference.

When comparing the stress σ_y between the thin and thick specimens, the thin specimen shows a more than 20 percent larger peak value of the stress at the crack tip element, as seen in Fig. 9. A delayed damage at the thin specimen allows more accumulation in the stress, and results in the higher peak stress. The delayed damage also yields a greater stress gradient very near the crack tip for the thin specimen than for the thick specimen at the applied strain levels for the maximum stresses. On the other hand, the strain ϵ_y at the crack tip element is almost the same for both thin and thick specimens until a small damage growth, but it is greater for the thick specimen after further damage growth.

The Crack Opening Displacement (COD) is quite uniform through the thickness of the thick and thin specimens, respectively. Thus, the COD criterion for the crack propagation also supports the uniform crack growth in the specimens as observed at the test. The COD at the same damage saturation level is plotted in Fig. 10. The plot shows almost the same COD for both the thin and thick specimens. This result indicates that the COD criterion can also predict the onset of crack growth at the same applied strain level for both thin and thick specimens.

The next study was for thin and thick specimens with a short

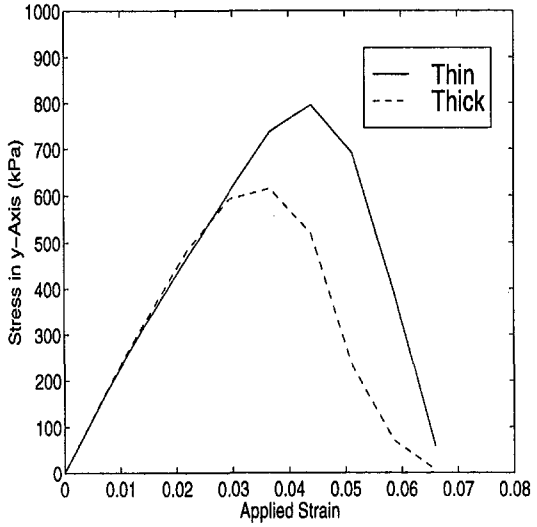

Fig. 9 Comparison of stress σ_y variation for thin and thick specimens with a long crack

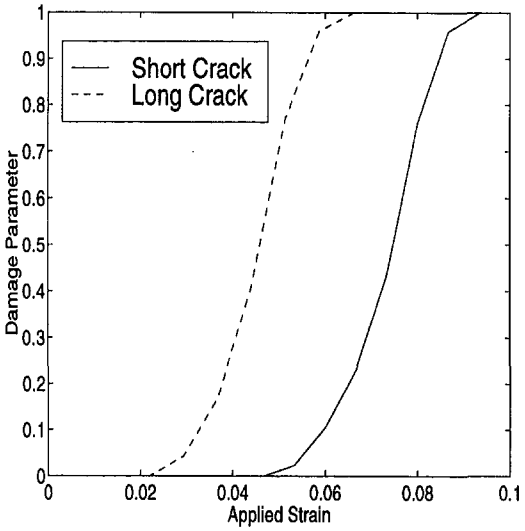

Fig. 11 Comparison of damage growth at crack tip elements of specimens with a short crack and a long crack

single edge crack. The crack tip of the short crack is close to the additional free surface, i.e., the left side yz-plane of the specimen as seen in Fig. 2. The additional free surface reduces the constraining effect around the crack tip compared to the long cracked specimen. For example, a measure for constraining effect, $\sigma_z/\{\nu(\sigma_x + \sigma_y)\}$, was computed at the center of the specimens with a short and a long crack. If the measure is close to zero, there is less constraint. For the long crack, the measure was 0.65 while it was 0.45 for the short crack. The less constraint as well as a smaller crack size delay the damage initiation near the crack tip compared to the long cracked specimen, as expected. The applied strain level for the damage initiation for the short cracked specimen is about twice of that for the long cracked specimen. However, once damage initiates, the additionally applied strain increment for damage saturation is approximately 15 percent greater for the short crack than for the long crack as seen in Fig. 11. Thus, the crack size and less constraint affect the damage initiation much more than the damage growth rate.

Figure 12 compares two thick specimens with a short and a long cracks. The long cracked specimen has a steeper increase of the stress σ_y at the crack tip element than the short cracked specimen at the same applied strain level until the applied strain reaches 3 to 4 percent. This is because of a higher stress intensity factor for the long crack before damage. Therefore, there is a delay in damage initiation for the short crack compared to the long crack. As the damage growth rate (damage increase per applied strain) is lower for the short crack, the stress at the short crack can reach the maximum value larger than that at the long crack. In other words, a faster damage growth in the long crack slows down the stress increase as the applied strain increases, and it lowers the peak stress level because the damaged material cannot support the stress any longer.

A lower constraint at the center of the specimen thickness near the short crack tip yields a smaller percentage of stress variation along the thickness compared to the variation in the long cracked specimen under the same applied strain until the strain becomes 3 percent where the stress becomes maximum at the center of the long crack. However, after peak stresses, the constraint effect becomes small at the center because of large damage, the stress drop rate (stress decrease per applied strain) is almost the same between the long and short cracks as seen in Fig. 12.

Figures 13 and 14 compare the damage contours between the

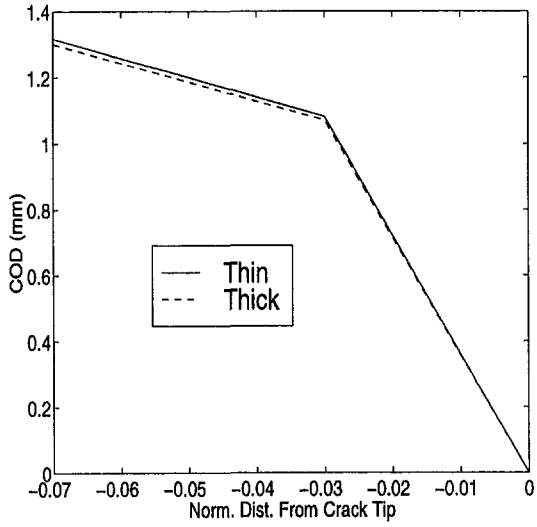

Fig. 10 Crack opening displacement of thin and thick specimens with a short crack

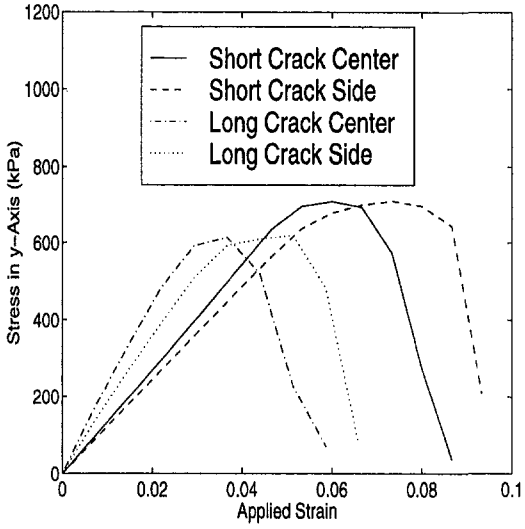

Fig. 12 Comparison of stress σ_y in thick specimens with a short crack and a long crack

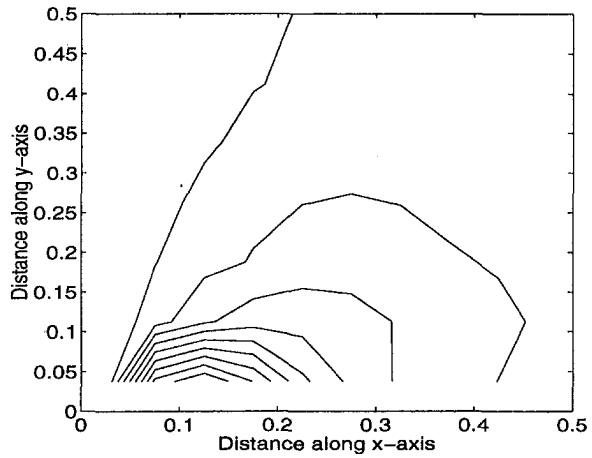

Fig. 13 Damage contours around the crack tip for thin specimen with a short crack at the applied strain level for damage saturation in the crack tip element: distances were normalized with respect to the specimen width. Contour lines are in 0.1 increment of the damage parameter.

short and long cracked specimens. Those figures are at the onset of damage saturation at the crack tip elements of the thin specimens, respectively. Therefore, the applied strain levels are different for the short and long cracked specimens. At the onset of damage saturation, the short crack has a slightly wider spread of damage from the crack tip. The contour shapes are very similar between the two specimens.

Conclusions

The numerical results agreed well with experimental observation. The damage saturation at the crack tip element (i.e., the onset of crack propagation) occurred at the same applied strain level for both thick and thin specimens. For the thick specimens, the damage saturation was uniform more than 90 percent of the thickness. Thus, uniform crack propagation through the thickness was predicted and observed for thick specimens.

The short crack had a long delay (about 100 percent larger applied strain) in damage initiation than the long crack, but the damage growth rate in the long crack was about 15 percent greater than the short crack. The slower damage growth in the short crack resulted in the higher maximum stress in σ_y. At the onset of damage saturation, the longer crack had slightly larger damage concentration around the crack tip.

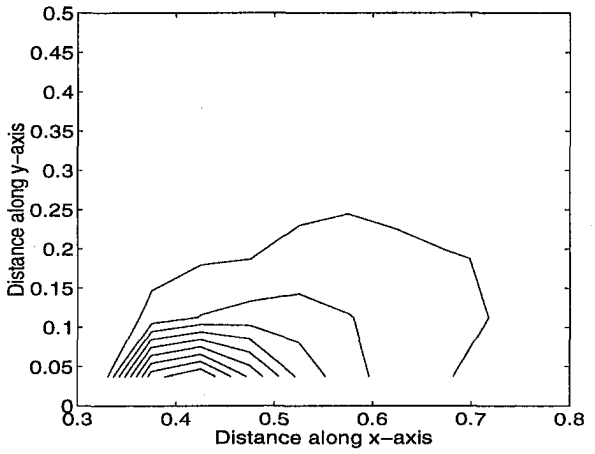

Fig. 14 Damage contours around the crack tip for thin specimen with a long crack at the applied strain level for damage saturation in the crack tip element: distances were normalized with respect to the specimen width. Contour lines are in 0.1 increment of the damage parameter.

References

Aboudi, J., 1987, "Closed Form Constitutive Equations for Metal Matrix Composites," *Int. J. Engng. Sci.,* Vol. 25, No. 9, pp. 1229–1240.

Aboudi, J., 1989, "Micromechanical Analysis of Composites by the Method of Cells," *Applied Mech. Rev.,* Vol. 42, No. 7, July, pp. 193–221.

Anderson, L. L., and Farris, R. J., 1988, "A Predictive Model for the Mechanical Behavior of Particulate Composites," *J. Polym. Engng. Sci.,* Vol. 28, pp. 522–528.

Cornwell, L. R., and Schapery, R. A., 1975, "SEM Study of Microcracking in Strained Solid Propellant," *Metallography,* Vol. 8, pp. 445–452.

Devries, F., Dumontet, H., Duvaut, G., and Lene, F., 1989, "Homogenization and Damage for Composite Structures," *Int. J. Num. Meth. Engng.,* Vol. 27, pp. 285–298.

Farris, R. J., 1968, "The Character of the Stress-Strain Function for Highly Filled Elastomers," *Trans. Soc. Rheol.,* Vol. 12, pp. 303–314.

Felice, G., and Rizzi, N., 1997, "Homogenization for Materials with Microstructure," *Recent Advances in Solids/Structures and Application of Metallic Materials,* eds., Y. W. Kwon, D. C. Davis, H. H. Chung, and L. Librecsu, ASME PVP-Vol. 369, pp. 33–38.

Gibson, R. F., 1994, *Principles of Composite Material Mechanics,* McGraw-Hill, New York.

Gurtin, M. E., Francis, E. C., 1981, "Simple Rate-Independent Model for Damage," *J. Spacecraft,* Vol. 18, No. 3, May–June, pp. 285–286.

Haj-Ali, R. M., 1996, "Hierarchical Material Models with Microstructure for Nonlinear Analysis of Progressive Damage in Laminated Composite Structures," Ph.D dissertation, University of Illinois at Urbana-Champaign.

Knauss, W. G., Palaniswamy, K., and Smith, G. C., 1973, "The Application of Rate Theory to the Failure of Solid Propellants," GALCIT SM Report 73-3, California Institute of Technology, Pasadena, CA.

Knott, J. F., 1973, *Fundamentals of Fracture Mechanics,* Butterworths, London, England.

Kwon, Y. W., 1993, "Calculation of Effective Moduli of Fibrous Composites with Micro-Mechanical Damage," *Composite Structures,* Vol. 25, pp. 187–192.

Kwon, Y. W., and Baron, D. T., 1998, "Numerical Predictions of Progressive Damage Evolution in Particulate Composites," *J. of Reinforced Plastics and Composites,* Vol. 17, No. 8, pp. 691–711.

Kwon, Y. W., Lee, J. H., and Liu, C. T., 1997, "Modeling and Simulation of Crack Initiation and Growth in Particulate Composites," ASME *Journal of Pressure Vessel Technology,* Vol. 119, August, pp. 319–324.

Kwon, Y. W., and Liu, C. T., 1997, "Study of Damage Evolution in Composites Using Damage Mechanics and Micromechanics," *Composite Structures,* Vol. 38, No. 1–4, pp. 133–139.

Liu, C. T., and Ravichandran, G., 1997, "An Experimental and Numerical Analysis of Near Tip Behavior in a Multi-Phase Material," *Recent Advances in Solids/Structures and Application of Metallic Materials,* Kwon, Y. W., Davis, D. C., Chung, H. H., and Librescu, L., eds., PVP-Vol. 369, ASME, New York, pp. 19–25.

Liu, C. T., and Smith, C. W., 1996, "Temperature and Rate Effects on Stable Crack Growth in a Particulate Composite Materials," *Experimental Mechanics,* Vol. 36, No. 3, September, pp. 290–295.

Murthy, P. L. N., and Chamis, C. C., 1984, "ICAN: Integrated Composite Analyzer," NASA TM-83700.

Pecknold, D. A., 1990, "A Framework for 3-D Nonlinear Modeling of Thick-Section Composites," David Taylor Research Center, DTRC-SME-90/92, October.

Pecknold, D. A., and Rahman, S., 1994, "Micromechanics-Based Structural Analysis of Thick Laminated Composites," *Computers and Structures,* Vol. 51, No. 2, pp. 163–179.

Ravichandran, G., and Liu, C. T., 1995, "Modeling Constitutive Behavior of Particulate Composites Undergoing Damage," *Int. J. Solids Structures,* Vol. 32, No. 6/7, pp. 979–990.

Renard, J., 1990, "Modeling of a Damaged Composite Specimen by a Micro-Macro Numerical Simulation," Composite Material Technology 1990, D. Hui and T. J. Kozik, eds., ASME PD-Vol. 32.

Schapery, R. A., 1982, "Models for Damage Growth and Fracture in Nonlinear Viscoelastic Composites," *Proc. 9th U.S. Natl. Cong. Appl. Mech.,* Pao, Y. H., ed., ASME, New York, pp. 237–245.

Shapery, R. A., 1986, "A Micromechanical Model for Non-linear Viscoelastic Behavior of Particle-Reinforced Rubber With Distributed Damage," *Engng. Fract. Mech.,* Vol. 25, pp. 845–867.

Schapery, R. A., 1991, "Analysis of Damage Growth in Particulate Composites Using a Work Potential," *Compos. Engng.,* Vol. 1, pp. 167–182.

Siboni, G., and Benveniste, Y., 1991, "A Micromechanics Model for the Effective Thermomechanical Behavior of Multiphase Composite Media," *Mechanics of Materials,* Vol. 11, pp. 107–122.

Simo, J. C., and Ju, J. W., 1987, "Strain- and Stress-based Continuum Damage Models—I. Formulation," *Int. J. Solids Structures,* Vol. 23, pp. 821–840.

Smith, C. W., Chang, C. W., and Liu, C. T., 1990, "Measurement of Crack Induced Damage in Particulate Composites," *Proc. of 1990 Annual Society for Experimental Mechanics,* pp. 241–246.